Automatic Identification of Internal Carotid Artery from 3DRA Images

Article *in* Conference proceedings: ... Annual International Conference of the IEEE Engineering in Medicine and Biology Society. IEEE Engineering in Medicine and Biology Society. Conference · August 2010

DOI: 10.1109/IEMBS.2010.5626473 · Source: PubMed

4 authors:

Hrvoje Bogunović
Medical University of Vienna
104 PUBLICATIONS **1,685** CITATIONS
SEE PROFILE

Jose Maria Pozo
University of Leeds
99 PUBLICATIONS **956** CITATIONS
SEE PROFILE

Rubén Cárdenes
HENSOLDT Sensors
71 PUBLICATIONS **731** CITATIONS
SEE PROFILE

Alejandro F Frangi
University of Leeds
689 PUBLICATIONS **17,541** CITATIONS
SEE PROFILE

Automatic Identification of Internal Carotid Artery from 3DRA Images

Hrvoje Bogunović, José María Pozo, Rubén Cárdenes and Alejandro F. Frangi

***Abstract*— Geometric characteristics and arrangement of the cerebral vessels are assumed to be related to the development of vascular diseases. Identifying anatomical segments and bifurcations of the cerebral vasculature allows the comparison of these characteristics across and within subjects. In this paper, we focus on the automatic identification of internal carotid artery (ICA) from 3D rotational angiographic images. The steps of the proposed method are the following: Arterial vascular tree is first segmented and centerlines are computed. From a set of centerlines, vascular tree topology is constructed and its bifurcations geometrically characterized. Finally, ICA terminal bifurcation is detected, which enables ICA identification. To detect ICA terminal bifurcation, a support vector machine classifier is trained. We processed 82 images to obtain 274 feature vectors of bifurcations around the ICA. 10×5-fold cross-validation showed an average accuracy of 99.6%, with 99.5% specificity and 100% sensitivity. The two most discriminating bifurcation features were: radius ratio between the smaller branch and its parent vessel, and the long-axis component of the smaller branch vector.**

I. Introduction

It has been postulated that geometric characteristics and arrangement of the cerebral vessels of the Circle of Willis may provide meaningful association with vascular disease formation and progression [1]. In particular, cerebral aneurysms (pathological dilation of the vessel) are frequently located at or near arterial bifurcations and after regions of high vascular curvature in arteries of the Circle of Willis [2]. Geometry of the parent vasculature was shown to have a profound impact on the intra-aneurysmal hemodynamic stresses (forces coming from blood motion), assumed to be related to the aneurysm risk of rupture [3].

However, there is still a lack of knowledge of the characteristic geometric features associated with cerebrovascular diseases and capable of distinguishing between healthy and diseased vasculature. Thus, there is a need to test the diagnostic and prognostic efficacy of these features through large-scale observational studies, processing hundreds or thousands of angiographic images [4].

To allow comparison of geometric features across and within subjects, the measurements have to be done on the corresponding anatomical segments of the vascular tree. Bifurcations constitute important landmarks for establishing the correspondence. Thus, two important operations required to compare the vasculature are landmark matching and anatomical labeling. These are tedious and time consuming tasks to be performed manually. Thus, automating these tasks becomes a crucial goal for large-case studies.

In this paper, we focus on automatic identification of internal carotid artery (ICA) from 3D rotational angiographic (3DRA) images by detecting its terminal bifurcation. ICA terminal bifurcation is an important anatomical landmark of the Circle of Willis and geometric characterization of ICA has recently been of great interest [5], [6], [7]. This case presents a paradigmatic application, but the presented framework could be applied to identify other vascular landmarks as well.

Located on each side of the neck, the ICA is the main vessel that feeds blood to the arteries forming anterior circulation of the brain. There are several bifurcations on the ICA before the terminal one, where it bifurcates into middle cerebral artery (MCA) and anterior cerebral artery (ACA). The ones most commonly visible in 3DRA images are ophthalmic artery (OA), posterior communicating artery (PcoA) and anterior choroidal artery (AchA) (Fig. 1).

Several works have been dealing with ICA characterization. In [5], the position and orientation of the aneurysm neck with respect to the ICA were quantified. In [6], they explored the relationship between geometric features of ICA and the aneurysm location. Lastly, in [7], a method is proposed for simultaneous alignment and clustering of the ICA centerline curves to differentiate between various types of carotid siphons. Although the above mentioned work relies on the use of ICA centerlines, the methods by which they were separated from the rest of the vascular tree, locating the ICA terminal bifurcation, were not explained.

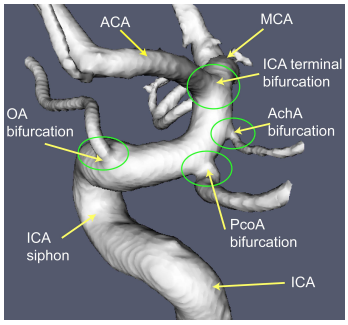

Fig. 1: Internal carotid artery and its main bifurcations.

This work was partially supported by the @neurIST Integrated Project (co-financed by the European Commission through the contract no. IST-027703), the CDTI CENIT-cvREMOD grant funded by the Spanish Ministry of Science and Innovation (MICINN-CDTI), the AGAUR-FI fellowship from Generalitat de Catalunya, and Philips Healthcare (Best, The Netherlands)

H. Bogunović, J. M. Pozo, R. Cárdenes and A. F. Frangi are with Center for Computational Imaging & Simulation Technologies in Biomedicine (CISTIB) - Universitat Pompeu Fabra (UPF) and Networking Biomedical Research Center on Bioengineering, Biomaterials and Nanomedicine (CIBER-BBN), Barcelona, Spain. A. F. Frangi is also with Institució Catalana de Recerca i Estudis Avançats (ICREA), Barcelona, Spain USA (e-mail: `alejandro.frangi@upf.edu`)

II. Methodology

3D rotational angiography (3DRA) acquisitions were performed with angiographic unit: Allura Xper FD20; Philips Healthcare, Best, The Netherlands. On a dedicated workstation, 3D images were reconstructed with a 256^3 matrix having a voxel size of $0.29 \times 0.29 \times 0.29$ (mm). Contrast injection was carried out to enhance the vessels comprising anterior cerebral circulation of either left or right hemisphere.

Segmentations of the vasculature were performed in an automated way with a geometric deformable model called Geodesic Active Regions (GAR) [8] and using an image intensity standardization technique [9]. The GAR method incorporates region descriptors together with image gradient magnitude to guide the evolution toward the vessel boundaries. The result of the segmentation is a triangular mesh modeling the vascular lumen.

A. Centerline computation

The vasculature segmented from 3DRA corresponds to the arterial tree. To construct its topology from the segmentation mesh, centerlines were first computed using the method introduced in [10] and implemented within VMTK library [11]. Centerline between two extremal points of the mesh is extracted as a minimal cost path along the Voronoi diagram constructed from the points of the segmentation mesh. Cost at each point of the path is defined as $F(x) = 1/R(x)$, where R is the radius of the maximally inscribed sphere. Centerlines of the vascular tree were extracted between pairs of points where one point always corresponded to the root of the tree while the other one was taken from a terminal leaf of the tree (Fig. 2(a)).

To automatically identify those points, we relied on the property that the mesh has open ends at the places where the vascular tree exits the field of view (FOV) used for the volume reconstruction. The root point was taken to be the center of mass of the largest contour of an open end at the lowest axial plane of the mesh, as it corresponds to a cross-section of ICA. The centers of mass of all the other open end contours were taken as terminal leaf end points.

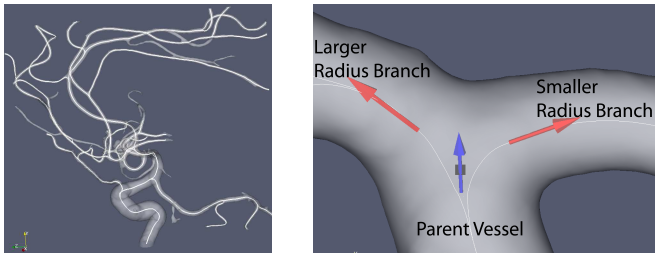

(a) (b)

Fig. 2: (a) Segmented mesh of the arterial tree and its centerlines. (b) Vessel bifurcation: Origin (black square) and associated bifurcation vectors (parent vessel vector and larger and smaller branch vectors).

B. Bifurcation analysis

From a set of centerlines, the topology was constructed with VMTK. Following the approach presented in [12], [5], to each centerline a tube surface is associated as a union (envelope) of maximally inscribed spheres whose centers lie on the centerline. Bifurcation is then defined as the region where tube surfaces of two centerlines join. Parent vessel and branches of each bifurcation (Fig. 2(b)) were identified which enabled the construction of the tree data structure (acyclic connected graph) where edges correspond to branches and nodes to bifurcations. In addition, geometric features of the bifurcations and branches were quantified: Bifurcation origin and vectors, as well as the mean vessel radii of the parent vessel and branches. We refer the reader to [12], [5] for more details on objective criteria used for defining the origin of a bifurcation and bifurcation vectors.

In order to identify ICA on the vascular tree, detecting its terminal bifurcation (where it branches into ACA and MCA) is sufficient. The ICA is then obtained by traversing the tree up until the root is reached. To detect this bifurcation, we applied a breadth-first search starting from the root. With this strategy we only needed to differentiate ICA terminal bifurcation from other bifurcations along the ICA as the potential error would appear either as a false positive along the ICA or a false negative at its terminal bifurcation.

We described each bifurcation with the following collection of features, similar to [13].

- Ratios of mean branch radii with respect to the parent vessel one: Larger radius branch and smaller radius branch defining larger radius ratio and smaller radius ratio, respectively.
- Sagittal, long-axis and coronal-components of the three bifurcation vectors: Parent vessel vector, larger branch vector and smaller branch vector.
- Angles between each pair of bifurcation vectors.

Hence, these features form a 14 dimensional bifurcation feature vector. Then, a machine learning based approach was applied, where a classifier was trained on a set of labeled bifurcation feature vectors to detect the ICA terminal bifurcation.

Using the sagittal component of the bifurcation vectors does not assure consistency when comparing left and right hemisphere bifurcations. Thus, for initial analysis purpose, all images of the left hemispheres were mirrored along the midsagittal plane to be comparable to the right ones.

C. Machine learning

Support vector machine (SVM) was employed for classification using LIBSVM package [14]. Two different kernels were tested. A linear one:

$$K(\vec{x}_i, \vec{x}_j) = \vec{x}_i^T \vec{x}_j \tag{1}$$

and a non-linear one where the training vectors x_i were mapped into a higher dimensional space where the inner product is computed by radial basis function (RBF) kernel:

$$K(\vec{x}_i, \vec{x}_j) = \exp(-\gamma \|\vec{x}_i - \vec{x}_j\|^2), \qquad \gamma > 0 \tag{2}$$

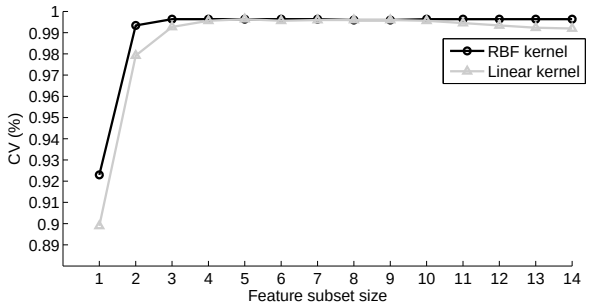

Fig. 3: CV accuracy for different feature subset sizes and the two kernel functions.

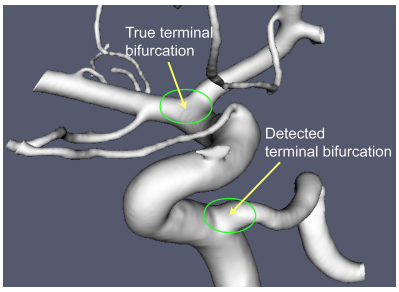

Fig. 4: Vasculature where the false positive case occurred. A bifurcation of ICA with a tentorial marginal branch, that is not commonly seen in 3DRA images, was mistaken for the terminal one.

SVM then finds a linear separating hyperplane with the maximal margin in this higher dimensional space. In general, the larger the margin the lower the generalization error of the classifier. The two classes were weighted, giving bigger penalty in the learning process if the class with fewer samples was misclassified and all the features were linearly scaled into range $[-1, 1]$. Optimal values for the penalty parameter C in the training error and the kernel parameter γ were obtained by a grid search through multiple combinations. For each choice of parameters, 5-fold cross validation (CV) was performed. This procedure was then repeated 10 times and the estimated accuracy of correct classification was taken as the average CV rate for all repetitions.

To optimize the performance of SVM we also performed feature selection. The purpose of feature selection was three-fold: reducing the dimensionality of data, potentially improving the predictive accuracy of the classifier and providing a better understanding of which are the most discriminating bifurcation features. Sequential forward selection (SFS) of features was used. Starting with an empty set at each forward (inclusion) step, the feature added to the feature subset is the one that maximizes the CV accuracy.

D. ICA identification

Once ICA terminal bifurcation is successfully detected, ICA centerline is extracted as a sequence of 3D points along a curvilinear abscissa starting from the terminal bifurcation of ICA (bifurcation with MCA and ACA) and proceeding toward the heart. Having ICA centerline differentiated from the others in the vascular tree, the segmented triangular mesh was labeled to designate the ICA.

III. Results

We have processed 82 images and in each image, we identified the terminal and $1-3$ non-terminal ICA bifurcations, which depended on whether bifurcations with PcoA and AchA were visible or not. Overall, feature vectors of 274 different bifurcations around ICA were extracted and labeled into two classes: terminal (82) and non-terminal (192).

The feature vectors were supplied to SVM classifier for training and cross-validation. The performance with respect to the chosen kernel function and the number of features selected is shown in Fig. 3.

SVM with RBF kernel function performed better than with the linear one. The maximum CV accuracy using linear kernel is reached with a subset having 5 features, while SVM with RBF kernel reached the same accuracy with only 3 features. As expected from the visual observation, the most discriminating feature was the smaller radius ratio. However, just thresholding based on that feature was clearly performing more poorly. Adding long-axis component of smaller branch vector increased the CV accuracy to 99.3%. Additionally appending coronal-axis component of parent vessel vector reached the maximum CV accuracy of 99.6% which was close to perfect classification: It had only one false positive and no false negatives. Hence, the specificity was 99.5% and the sensitivity was 100%, which shows that the chosen features describe well the bifurcation. Furthermore, the false positive sample (Fig. 4) was the only example of such a bifurcation available, hence during its testing none were present in the training data.

To have a better idea how the samples were separated we plotted the result for 2D feature subset formed by smaller radius ratio and long-axis component of smaller branch vector (Fig. 5). Large value of the long-axis component meant that the vector was pointing toward the tip of the head.

SVM parameter sensitivity analysis, for the case of 14 features with RBF kernel, (Fig. 6) revealed a plateau of values where CV $> 99\%$. Hence, the parameters chosen were not critical. Finally, as an example of the results of the proposed method we show a set of segmented meshes with ICA successfully identified (Fig. 7).

IV. Conclusions

We have presented an automatic method for ICA identification by characterizing and detecting its bifurcation with ACA and MCA in the vascular tree. The two features that contributed the most to the ICA terminal bifurcation distinction were: *ratio of mean radii between the smaller branch and its parent vessel* and *long-axis component of the smaller branch vector*. As they are invariant to the circulation side (left or right) mirroring, the classification based on these features gives a completely automatic method, not requiring any user defined parameter.

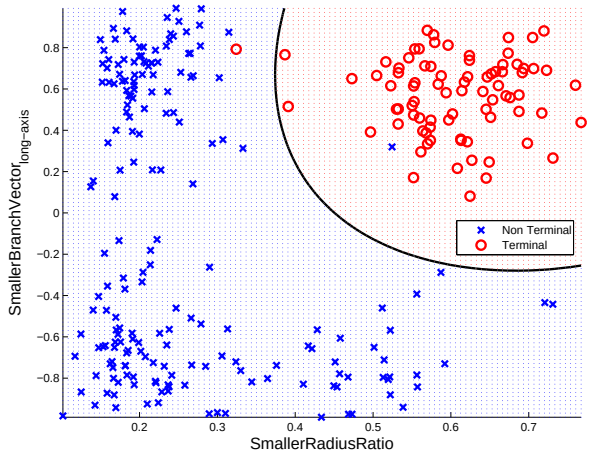

Fig. 5: Classification with SVM in 2D feature space using RBF kernel. Features shown are the two that were giving the highest CV rate. The classifier trained in this 2D space misclassified one vector of each class.

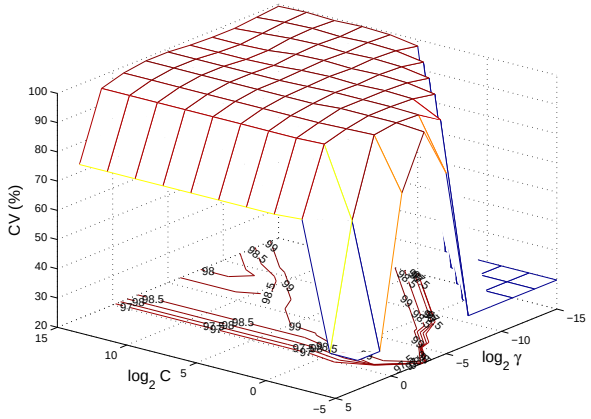

Fig. 6: Sensitivity of CV accuracy to the parameters chosen for SVM with RBF kernel.

Relying on the long-axis component of the bifurcation vector as a feature does introduce a limitation: the method is sensitive to the tilting of the patient's head. Thus, these features would not be consistent with the ones of the training set. Nevertheless, imaging with patient's head tilted is rarely performed.

In the future work, we plan to extend the proposed method to identify other vascular segments and bifurcations in the Circle of Willis as well as apply it to ICA geometric characterization and variability analysis from a large number of images.

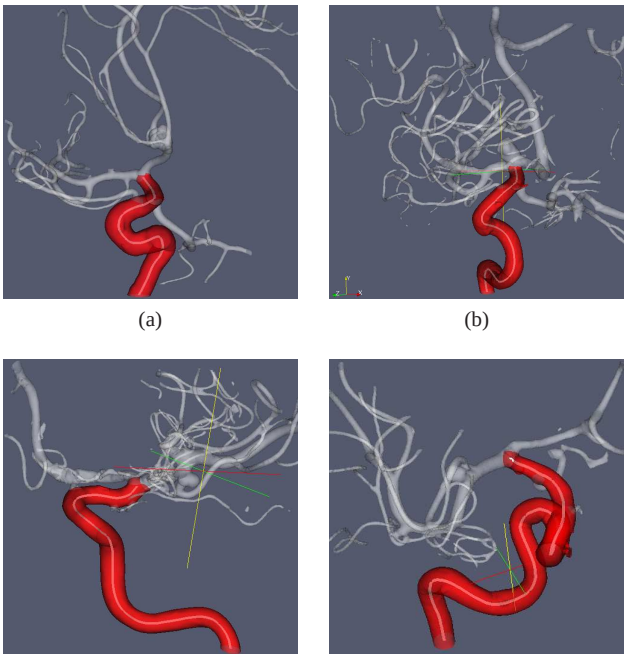

Fig. 7: Set of identified ICA and their centerlines.

REFERENCES

[1] N. K. Rooij, B. K. Velthuis, A. Algra, and G. J. E. Rinkel, "Configuration of the circle of Willis, direction of flow, and shape of the aneurysm as risk factors for rupture of intracranial aneurysms," *J. Neurol.*, vol. 256, no. 1, pp. 45–50, Jan. 2009.

[2] J. L. Brisman, J. K. Song, and D. W. Newell, "Cerebral aneurysms," *N. Engl. J. Med.*, vol. 355, no. 9, pp. 928–939, Aug. 2006.

[3] J. R. Cebral, M. A. Castro, J. E. Burgess, R. S. Pergolizzi, M. J. Sheridan, and C. M. Putman, "Characterization of cerebral aneurysms for assessing risk of rupture by using patient-specific computational hemodynamics models," *AJNR Am. J. Neuroradiol.*, vol. 26, no. 10, pp. 2550–2559, 2005.

[4] S.-W. Lee, L. Antiga, J. D. Spence, and D. A. Steinman, "Geometry of the carotid bifurcation predicts its exposure to disturbed flow," *Stroke*, vol. 39, no. 8, pp. 2341–2347, 2008.

[5] M. Piccinelli, A. Veneziani, D. A. Steinman, A. Remuzzi, and L. Antiga, "A framework for geometric analysis of vascular structures: application to cerebral aneurysms." *IEEE Trans. Med. Imag.*, vol. 28, no. 8, pp. 1141–1155, Aug. 2009.

[6] L. M. Sangalli, P. Secchi, S. Vantini, and A. Veneziani, "A case study in exploratory functional data analysis: Geometrical features of the internal carotid artery," *J. Am. Stat. Assoc.*, vol. 104, no. 485, pp. 37–48, 2009.

[7] L. M. Sangalli, P. Secchi, S. Vantini, and V. Vitelli, "K-mean alignment for curve clustering," *Comput. Stat. Data Anal.*, vol. 54, no. 5, pp. 1219–1233, May 2010.

[8] M. Hernandez and A. F. Frangi, "Non-parametric geodesic active regions: method and evaluation for cerebral aneurysms segmentation in 3DRA and CTA," *Med. Image Anal.*, vol. 11, no. 3, pp. 224–241, Jun. 2007.

[9] H. Bogunovic, A. G. Radaelli, M. De Craene, D. Delgado, and A. F. Frangi, "Image intensity standardization in 3D rotational angiography and its application to vascular segmentation," in *Proc. SPIE Med. Imag.*, J. M. Reinhardt and J. P. W. Pluim, Eds., vol. 6914, 2008, article 691419.

[10] L. Antiga, B. Ene-Iordache, and A. Remuzzi, "Computational geometry for patient-specific reconstruction and meshing of blood vessels from MR and CT angiography," *IEEE Trans. Med. Imag.*, vol. 22, no. 5, pp. 674–684, May 2003.

[11] L. Antiga and D. A. Steinman, "VMTK: the Vascular Modeling Toolkit." 2010. [Online]. Available: http://www.vmtk.org

[12] ——, "Robust and objective decomposition and mapping of bifurcating vessels." *IEEE Trans. Med. Imag.*, vol. 23, no. 6, pp. 704–713, Jun. 2004.

[13] J. B. Thomas, L. Antiga, S. L. Che, J. S. Milner, D. A. H. Steinman, J. D. Spence, B. K. Rutt, and D. A. Steinman, "Variation in the carotid bifurcation geometry of young versus older adults: implications for geometric risk of atherosclerosis," *Stroke*, vol. 36, no. 11, pp. 2450–2456, 2005.

[14] C.-C. Chang and C.-J. Lin, *LIBSVM: a library for support vector machines*, 2001. [Online]. Available: http://www.csie.ntu.edu.tw/~cjlin/libsvm